

Ion irradiation of crystalline H₂O–ice: Effect on the 1.65- μ m band

Rachel M.E. Mastrapa^{a,*}, Robert H. Brown^b

^a *Astrophysics Branch, NASA Ames Research Center, Mail Stop 245-6, Moffett Field, CA 94035-1000, USA*

^b *Department of Planetary Sciences, The University of Arizona, Tucson, AZ 85721, USA*

Received 6 December 2005; revised 14 February 2006

Available online 17 April 2006

Abstract

We have found that 0.8 MeV proton irradiation of crystalline H₂O–ice results in temperature dependent amorphization. The H₂O–ice’s phase was determined using the near infrared spectrum from 1.0 μ m (10,000 cm⁻¹) to 2.5 μ m (4000 cm⁻¹). In crystalline H₂O–ice, the 1.65- μ m (6061 cm⁻¹) band is strong while it is nearly absent in the amorphous spectrum [Schmitt, B., Quirico, E., Trotta, F., Grundy, W.M., 1998. In: Schmitt, B., de Bergh, C., Festou, M. (Eds.), *Solar System Ices*. Kluwer Academic, Norwell, MA, 1998, pp. 199–240]. In this experiment, at low temperatures (9, 25, and 40 K), irradiation of crystalline H₂O–ice produced the amorphous H₂O–ice’s spectrum. However, at 50 K, some crystalline absorptions persisted after irradiation and at 70 and 100 K the crystalline spectrum showed only slight changes after irradiation. Our results agree with previous H₂O–ice irradiation studies examining the crystalline peaks near 44 and 62 μ m by Moore and Hudson [Moore, M.H., Hudson, R.L., 1992. *Astrophys. J.* 401, 353–360] and near 3.07 μ m by Strazzulla et al. [Strazzulla, G., Baratta, G.A., Leto, G., Foti, G., 1992. *Europhys. Lett.* 18, 517–522] and by Leto and Baratta [Leto, G., Baratta, G.A., 2003. *Astron. Astrophys.* 397, 7–13]. We present a method of measuring band areas to quantify the phase and radiation dose of icy Solar System surfaces.

© 2006 Elsevier Inc. All rights reserved.

Keywords: Ices; Infrared observations; Kuiper belt objects; Radiation chemistry; Spectroscopy

1. Introduction

The observation of crystalline H₂O–ice on Quaoar (Jewitt and Luu, 2004) has continued the debate about the stability of amorphous and crystalline H₂O–ice in the outer Solar System. This result is particularly interesting because, due to the phase of the ice, the surface of Quaoar is interpreted to be young even though it is in a hypothetically primordial environment. This interpretation is based on assumptions about the dominant processes occurring on the objects surface, including radiation effects. Remote detection of the phase and temperature of H₂O–ice is possible by conducting observations in the infrared spectrum and comparing them to known samples in the lab. The near-infrared, 1–3 μ m, is especially relevant to outer Solar System objects due to the reflected light flux and the windows through atmospheric absorptions. We add to previous

results to refine the interpretation of H₂O–ice’s near-infrared spectrum. To review this model, we will discuss the phase stability of H₂O–ice on airless bodies, the infrared spectrum of H₂O–ice, the phase and temperature dependence of that spectrum, and the effects of irradiation on H₂O–ice phase.

The phase of H₂O–ice is dependent on the pressure and temperature conditions at the time of formation, and the temperature history of the ice. On the surfaces of outer Solar System objects, H₂O forms a solid that is either in an amorphous phase (*Ia*) or in one of two crystalline phases: cubic (*Ic*) or hexagonal (*Ih*) (Cruikshank et al., 1998; Jenniskens et al., 1998; Schmitt et al., 1998). Amorphous H₂O–ice converts to the cubic phase in an exothermic reaction near 135 K (Jenniskens and Blake, 1994; Kouchi et al., 1994; Sugisaki et al., 1969). The cubic phase of H₂O–ice, *Ic*, is a metastable version of *Ih* found in the laboratory at temperatures between 135 and 170 K (Jenniskens et al., 1997; Petrenko and Whitworth, 1999; Sugisaki et al., 1969). H₂O–ices above 170 K are hexagonal in phase (*Ih*). Based on the phase stability of H₂O–ice, the presence of amorphous H₂O–ice on a surface means that the surface has been colder than 135 K since formation.

* Corresponding author. Fax: +1 604 604 6779.

E-mail addresses: rmastrapa@arc.nasa.gov, mastrapa@lpl.arizona.edu (R.M.E. Mastrapa).

Table 1
Amorphous H₂O–ice infrared bands

Peak position cm ⁻¹ (μm)	A (cm/molecule)	Assignment	Temperature (K)	Reference ^a
6684 (1.496)	$(8.8 \pm 1.0) \times 10^{-19}$	2ν ₃	10	1
5040 (1.984)	$(1.2 \pm 0.1) \times 10^{-18}$	ν ₂ + ν ₃	10	1
3280 (3.045)	2.0×10^{-16}	ν ₁	14	2
1660 (6.024)	1.2×10^{-17}	ν ₂	14	2
760 (13.16)	3.1×10^{-17}	ν _R	14	2

^a 1. 10 K (Gerakines et al., 2005). 2. 14 K (Gerakines et al., 1995).

Table 2
Amorphous H₂O–ice bands at 10 K from Hudgins et al. (1993)

Peak position cm ⁻¹ (μm)	A (cm/molecule)
3298 (3.032)	1.7×10^{-16}
2202 (4.541)	3.3×10^{-18}
1657 (6.035)	1.0×10^{-17}
760 (13.15)	2.8×10^{-17}
211 (47.39)	4.2×10^{-18}

H₂O–ice is detected on Solar System objects by its distinctive infrared absorptions caused by inter- and intra-molecular vibrations. For clarity, we divide the infrared spectrum into three regions: the near-infrared or NIR (1–2.5 μm, 10,000–4000 cm⁻¹), the mid-infrared or MIR (2.5–10 μm, 4000–1000 cm⁻¹), and the far-infrared or FIR (10–100 μm, 1000–100 cm⁻¹). Due to the reflected flux of infrared light and windows in the Earth's atmosphere, the majority of ground-based observations of Solar System objects are in the NIR. These bands are overtones and combinations of vibrations found at longer wavelengths (Gerakines et al., 2005; Hudgins et al., 1993; Ockman, 1958). Tables 1 and 2 list the band positions, assignments, and A-values for the main H₂O–ice features, including those at longer wavelengths (Gerakines et al., 1995). The A-values, or the integrated band strength divided by column density, are included to demonstrate that the NIR features are by far the weakest of all of the H₂O–ice infrared bands.

Although the cubic and hexagonal phases of solid H₂O have identical infrared spectra (Bertie and Whalley, 1967), the spectra of amorphous and crystalline H₂O–ices are easily distinguishable at all wavelengths (Bertie and Whalley, 1964; Hagen and Tielens, 1982; Hagen et al., 1981; Ockman, 1958; Smith et al., 1994; Whalley, 1977). The infrared bands are stronger and sharper in the crystalline phase than those in the amorphous phase (Schmitt et al., 1998). We will expand on these distinctions in Section 3. The infrared spectrum of H₂O–ice is also strongly temperature dependent (Bertie and Whalley, 1967; Smith et al., 1994; Hagen and Tielens, 1982). There is a strong inverse correlation between temperature and the strength of the 1.65-μm H₂O–ice peak (Fink and Larson, 1975; Grundy and Schmitt, 1998). In monocrystalline samples, as temperature increases, the bands at 1.5-, 1.56-, 1.65-, and 2-μm all shift to shorter wavelengths, and the absorptions at 1.56 and 1.65 μm lose intensity (Grundy and Schmitt, 1998).

Lacking an atmosphere, the surfaces of many Solar System bodies experience a high flux of energetic particles. Radiation can initiate chemical reactions in exposed ices producing com-

plex organics (Bernstein et al., 2002; McDonald et al., 1996; Schutte et al., 1993). Several groups have looked at the radiation effects in H₂O– and D₂O–ices, such as the amorphization of crystalline bands, chemical changes, and the escape of materials (Bednarek et al., 1998; Brown et al., 1982; Ciavola et al., 1982; Hase and Kawabata, 1976; Johnson and Moulton, 1978; Kouchi and Kuroda, 1990; Moore and Hudson, 1992; Reimann et al., 1984; Siegel et al., 1961; Strazzulla et al., 1991b; Watanabe et al., 2000). We will concentrate on the amorphization of crystalline H₂O–ice seen in ion irradiation in the MIR (Leto and Baratta, 2003; Strazzulla et al., 1991a, 1992), FIR (Moore and Hudson, 1992), and UV photolysis of the MIR (Leto and Baratta, 2003) and XRD spectra (Kouchi and Kuroda, 1990), although the dose of the XRD results has been called into question (Jenniskens et al., 1995). One other measurement of amorphization has been made in the NIR (Leto et al., 2005) at only one temperature: 90 K. We expand on their result by irradiating crystalline H₂O–ice at a range of temperatures to see if the amorphization is temperature dependent.

If we can place constraints on the temperature and radiation history of an object in the Solar System, we may be able to estimate the age of a given surface by determining the phase of H₂O–ice on the surface. This estimate would be a result of balancing the dominant processes on the surface of these objects, including irradiation, impact-heating, and thermal variations, all of which are relevant on the surfaces of Kuiper Belt Objects, e.g., (Stern, 2003). We contribute to this model by measuring the doses needed to amorphize crystalline H₂O–ice in the NIR.

2. The experiment

The laboratory equipment used for this work has been described previously (Moore and Hudson, 1992). In the system schematic (Fig. 1), H₂O–vapor was introduced into the sample chamber to produce thin films of H₂O–ice on an aluminum mirror. The minimum temperature and pressure, 9 K and 9×10^{-8} Torr, respectively, were achieved using a Varian Turbo-V 250 mini-pumping station and a closed-cycle helium cooler (APD Cryogenics INC). The temperature of the mirror was maintained to ± 1 K by a Scientific Instruments temperature controller connected to a heating coil right above the mirror (Moore et al., 1983).

An infrared spectrometer (Bruker Vector 22) was connected to the sample chamber so that the IR beam passed into the system, reflected off the mirror and the sample, and returned into the spectrometer. All spectra were collected averaging 200 scans over the range 2000–8000 cm⁻¹ at a resolution of 4 cm⁻¹.

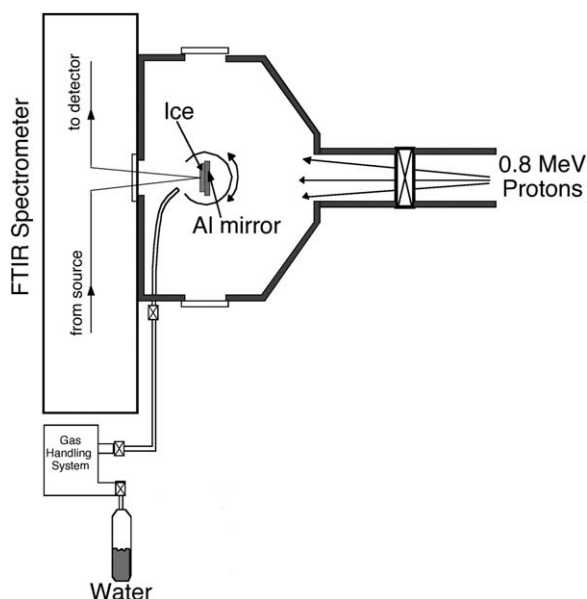


Fig. 1. Schematic of the Extraterrestrial Ice Lab at NASA/Goddard Space Flight Center. H₂O vapor is introduced into the chamber where it deposits on the sample mirror. The sample can be rotated to face either the infrared spectrometer for measurements or the van de Graaff accelerator for irradiations.

The aluminum mirror was polished for high reflectivity on one side, while the other side was anodized, providing low thermal resistivity and high electrical resistivity (Moore et al., 1983). The substrate was rotated into the beam path of a Van de Graaff generator, which was the source of 1-MeV protons. The beam passed through a nickel foil that prevented contamination from the Van de Graaff chamber and reduced the initial 1-MeV energy of the beam to 0.8-MeV (Moore et al., 1983). The number of protons incident on the sample was measured by an electrometer connected to the sample mirror, which was electrically isolated from the rest of the system. We calculated the dose in eV/molecule by multiplying the stopping power of 0.8 MeV protons in H₂O-ice [381 MeV cm²/g or 11.4 eV cm² 10⁻¹⁵/molecule (Northcliffe and Shilling, 1970)], by the direct measurement of the number of protons incident on the sample (p⁺/cm²).

For all experiments the range of doses was from 5×10^{13} to 1.4×10^{15} p⁺/cm² or 0.6–16 eV/molecule. We performed background experiments to confirm that the amount of contamination that accumulated in the chamber during a typical experiment was negligible. We prepared H₂O-ice samples from a liquid-H₂O sample with a resistivity of 18.2 MΩ cm. The liquid-H₂O was degassed using several freeze-thaw cycles with liquid N₂ and a mechanical pump. When introduced to the sample chamber, the H₂O-vapor formed a thin film on the pre-cooled aluminum substrate. We measured sample thickness with a laser beam that passed through the sample and reflected off the mirror to a detector. As the sample grew we counted the interference fringes and calculated the thickness using the following equation: $t = m\lambda/2n$, where t is the estimated sample thickness, m is the number of fringes, λ is the wavelength of the laser (0.67 μm), and n is the index of refraction of H₂O-ice (1.32) (Heavens, 1991). The fringes quickly damped down to an

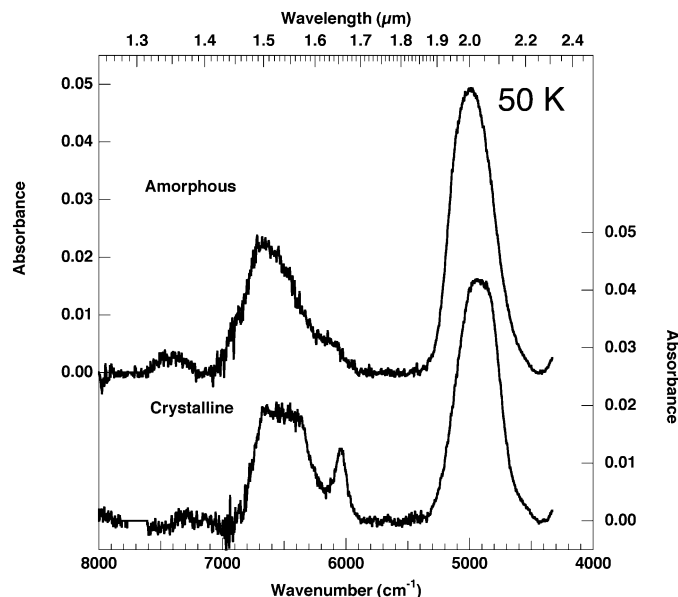


Fig. 2. Absorbance spectra of the amorphous and crystalline phases of the same H₂O-ice sample at 50 K. The sample was deposited in the amorphous phase at 50 K, heated to 160 K to crystallize, and cooled back to 50 K. The 1.65-μm band is very strong in the spectrum of crystalline H₂O-ice, but is only a weak shoulder in the spectrum of amorphous H₂O-ice. The spectra are stacked for clarity.

undetectable level, and so we used the rate of deposition for the first five fringes and timed the remainder of the sample deposition. This leads to a large estimated error in the thickness of the sample, but since the thickness of the sample was not needed for analysis of the data, we accepted this high error. To balance the time it takes to deposit a sample with the increase in strength of the bands with sample thickness, we decided to use a thickness of 30 fringes, or 8 ± 1.5 μm, for all of the experiments. We did not expect the sample to be heated by irradiation because the majority of thermal energy is deposited in the last 5% of an ion's path (Johnson, 1982), and the thickness of our samples are only about 50% of the penetration depth of 0.8 MeV protons in H₂O-ice (~16 μm) (Northcliffe and Shilling, 1970). Also, previous experiments with identical equipment detected no measurable change in temperature with irradiation (Hudson and Moore, 1992).

3. Results and analysis

3.1. Change with phase and temperature

The spectra of the amorphous and crystalline phases of an H₂O-ice sample deposited at 50 K are easily distinguished (Fig. 2). The changes with phase seen in these spectra agree with previous measurements (Schmitt et al., 1998). The most striking difference is the strength and sharpness of the 1.65-μm band in the crystalline-ice spectrum compared to its appearance as a broad shoulder in the amorphous-ice spectrum. The other H₂O-ice features are affected by phase, but not as strongly as the 1.65-μm band. Qualitatively, the H₂O-ice absorptions appear shifted to slightly longer wavelength in the crystalline-ice spectrum, compared to the amorphous-ice spectrum. Also, all

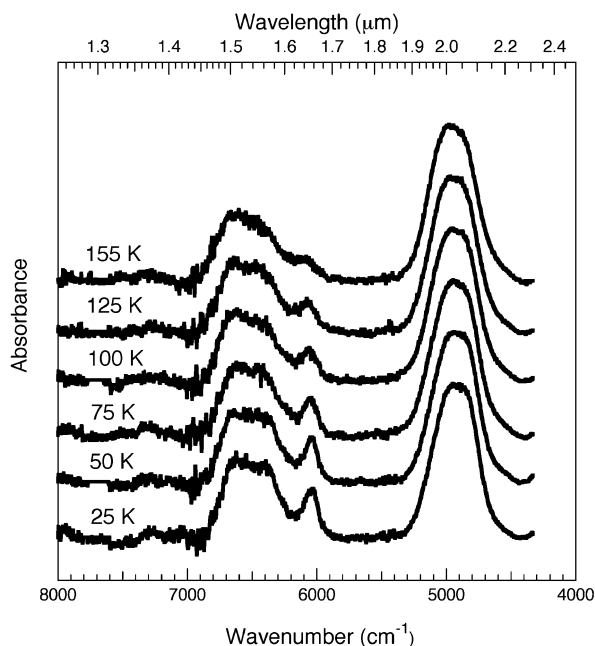


Fig. 3. Absorbance spectra of crystalline H₂O-ice deposited at 50 K and heated to 155 K for crystallization. The spectra were taken while cooling the ice. As the ice cooled the 1.65- μm feature grew stronger. The spectra are stacked for clarity.

of the features in the crystalline-ice spectrum are stronger and sharper than those in the amorphous-ice spectrum. The one exception to this pattern is the 2- μm band, which is stronger and sharper in the amorphous-ice spectrum.

The NIR features of crystalline-ice spectra are strongly temperature dependent (Fig. 3). The most obvious change is that of the 1.65- μm band, which grows stronger and sharper as the sample is cooled. Also, the 1.65- μm band also grows weaker when the sample is heated, demonstrating the reversibility of this process. These changes are consistent with those seen previously (Clark, 1981; Grundy and Schmitt, 1998; Hapke et al., 1981; Schmitt et al., 1998). In contrast, the combination modes in the spectra of amorphous-phase H₂O-ice only display slight changes with temperature (Fig. 4).

We measured the changes in peak center for the 2- μm band for amorphous and crystalline H₂O-ices at a range of temperatures from 9 to 150 K (Fig. 5). All of these measurements were made from a single experiment with a sample deposited at 90 K. The center of the 2- μm feature is strongly temperature dependent in the spectra of crystalline H₂O-ice while it is independent of temperature in amorphous-ice spectra. This temperature dependence in crystalline H₂O-ice is also reversible. The 2- μm peak in amorphous H₂O-ice is shifted from the peak center of the crystalline-ice spectrum by $\sim 130\text{ cm}^{-1}$. This large shift in peak center is a useful diagnostic tool for identifying the phase of H₂O-ice. Unfortunately, the noise in the spectra of H₂O-ice deposited at temperatures lower than 40 K was too high to accurately measure the peak center. We list peak centers from the 90 K experiment with phase and temperature in Table 3.

To attempt to quantify the changes between the amorphous and crystalline H₂O-ice we measured the area of the bands in two regions. First we measured the total area of the fea-

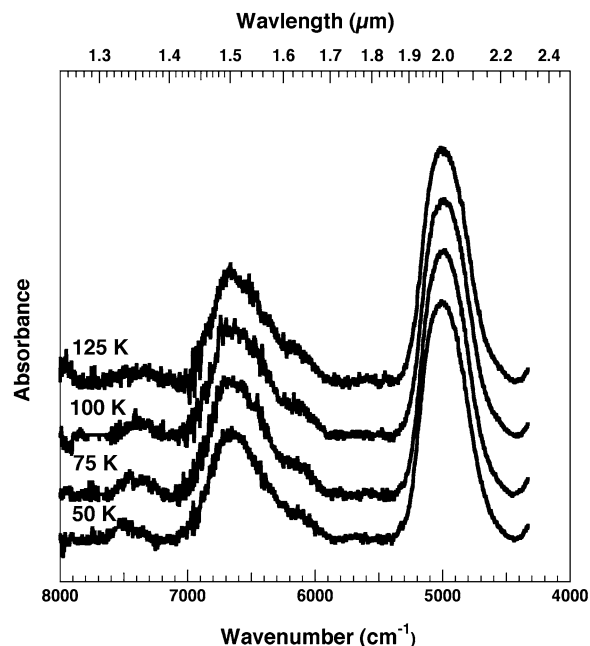


Fig. 4. Absorbance spectra of amorphous H₂O-ice deposited at 50 K and heated to 75, 100, and 125 K. There are almost no clear changes in the features with temperature. The spectra are stacked for clarity.

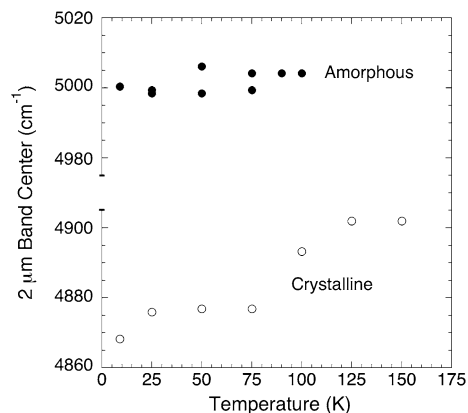


Fig. 5. Change in the center of the 2- μm band with phase and temperature. Amorphous (closed circles) crystalline (open circles). The H₂O-ice sample was deposited at 90 K. Note that the y-axis is broken to bring the two plots closer together.

tures from 1.42 to 1.72 μm . We named this region the “big 1.5”- μm band, since it includes the features at 1.5, 1.56, and 1.65 μm . We then measured the area of the 1.65- μm feature from 1.60 to 1.72 μm . We estimated the error in these areas by measuring the area of a spectrum with no sample. Finally, we divided the area of the 1.65- μm band by the area of the “big 1.5”- μm band. We differ in the calculation of the 1.65- μm band area from previous measurements (Fink and Larson, 1975; Grundy and Schmitt, 1998; Leto et al., 2005) in that we use the same baseline for both the 1.65- μm band and the “big 1.5”- μm band instead of drawing the baseline along the slope underneath the 1.65- μm band. We do not use this method for two reasons: (1) the error in the measurement is larger than the 1.65- μm band area and (2) small changes in selecting the anchor points of

Table 3
Near-infrared amorphous (*I_a*) and crystalline (*I_c*) H₂O-ice bands deposited at 90 K

Phase	Temperature (K)	Peak position cm ⁻¹ (μm)			
<i>I_a</i>	9	6630 (1.508)	–	6075 (1.646)	5007 (1.998)
<i>I_c</i>	9	6657 (1.502)	6378 (1.568)	6045 (1.654)	4868 (2.054)
	25	6658 (1.502)	6387 (1.566)	6045 (1.654)	4876 (2.051)
	50	6659 (1.502)	6389 (1.565)	6049 (1.653)	4877 (2.050)
	75	6661 (1.501)	6389 (1.565)	6060 (1.650)	4877 (2.050)
	100	6665 (1.500)	6415 (1.559)	6063 (1.649)	4893 (2.044)
	125	6668 (1.500)	6414 (1.559)	6073 (1.647)	4902 (2.040)
	150	6671 (1.499)	6423 (1.557)	6075 (1.646)	4902 (2.040)

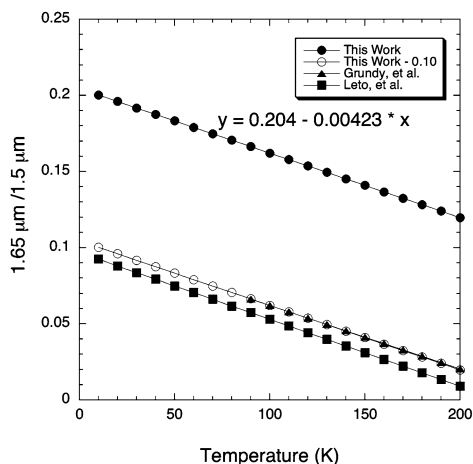


Fig. 6. Comparison of a fit of our method of calculating the ratio of the 1.65- and “big 1.5”-μm bands (filled circles) with fits of Grundy and Schmitt (1998) (filled triangles) and Leto et al. (2005) (filled squares). If we subtract 0.10 from our fit (open circles), we achieve good agreement with Grundy and Schmitt’s results and it is slightly higher than Leto et al.’s results. Grundy and Schmitt’s results diverge significantly from ours at low temperature (not shown) because they model a variety of grain sizes.

the baseline lead to very large changes in area. Since the areas are already very small, the tiny changes involved in selecting different baselines are magnified. We eliminate this error by using the same baseline for the measurement of both band areas. We compared a fit of our crystalline H₂O-ice results with those published previously and show that we can reproduce the slope of the line at a higher y-intercept (Fig. 6). Essentially, our results are exactly the same as previous work with an offset of 0.1. We encourage future observers to use either method and simply add or subtract the offset for comparison.

We plotted the 1.65-“big 1.5” ratio against temperature and showed that there is a clear difference between amorphous and crystalline H₂O-ice (Fig. 7). The errors are generally smaller than the data points and always smaller than the scatter between experiments, so we removed the error bars from the figure for clarity. The crystalline phase is strongly temperature dependent, while the results from the amorphous phase are too scattered to produce any trend. As temperature increases the phases become closer in ratio until they are indistinguishable at 170 K. This is a useful quantitative measurement to differentiate between the phases, but it does not fully represent the qualitative changes seen in the spectra at high temperatures. Our results

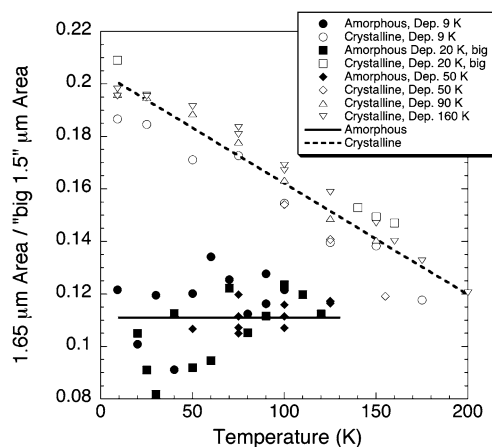


Fig. 7. H₂O-ice’s changes with phase and temperature represented by the ratio of areas of the 1.65-μm band to the “big 1.5”-μm band. See the text for the definition of the “big 1.5”-band. Empty and filled symbols correspond to crystalline and amorphous H₂O-ice, respectively. These data were collected from five different experiments where the samples were deposited at 9 K (circles), 20 K (squares), 50 K (diamonds), 90 K (triangles), and 160 K (inverted triangles). The solid line is the average value of the amorphous data while the dashed line is a linear best fit of the crystalline data.

produce the same behavior that earlier studies have found but at a higher scale due to the difference in area calculation (Grundy and Schmitt, 1998; Leto et al., 2005).

3.2. Change with dose

We irradiated crystalline H₂O-ice samples with 0.8 MeV protons at 9, 25, 40, 50, 70, and 100 K. As in previous experiments (Moore and Hudson, 1992; Strazzulla et al., 1992), the amorphization of crystalline H₂O-ice is temperature dependent. At 9, 25, and 40 K, the irradiated spectrum is almost indistinguishable from the amorphous spectrum (Fig. 8). At higher temperatures, 50, 70, and 100 K, the crystalline character of the absorptions remain in the spectrum (Fig. 9). No new features were seen in the irradiated spectra.

To compare the irradiation results between experiments, we again divided the area of the 1.65-μm band by that of the “big 1.5”-μm band (Fig. 10). The lines on the figure connect samples from different experiments that have been exposed to the same dose, while the points at the same temperature represent an individual experiment. As the dose increases, the ratio in all experiments moved closer to the amorphous line. Using this tool to

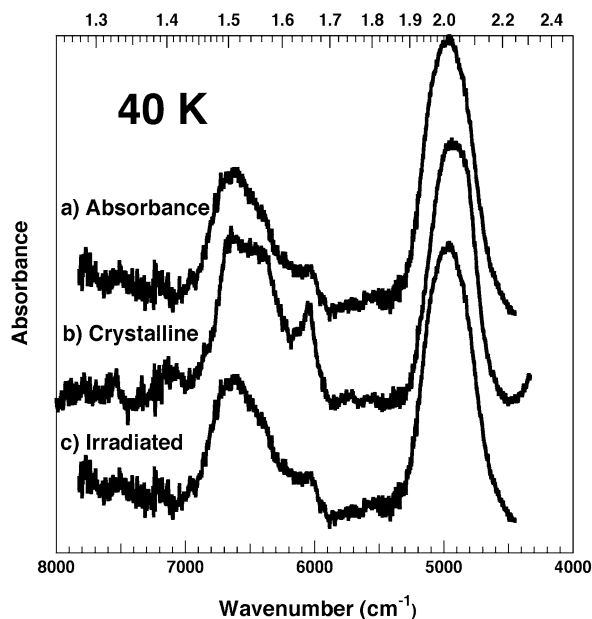


Fig. 8. Absorbance spectra of an H₂O–ice sample deposited at 40 K (a), heated to 160 K, and cooled to 40 K (b) before irradiating to a dose of 13 eV/molecule (c). Irradiation reduces the strength of the 1.65- μ m band. The spectra are stacked for clarity.

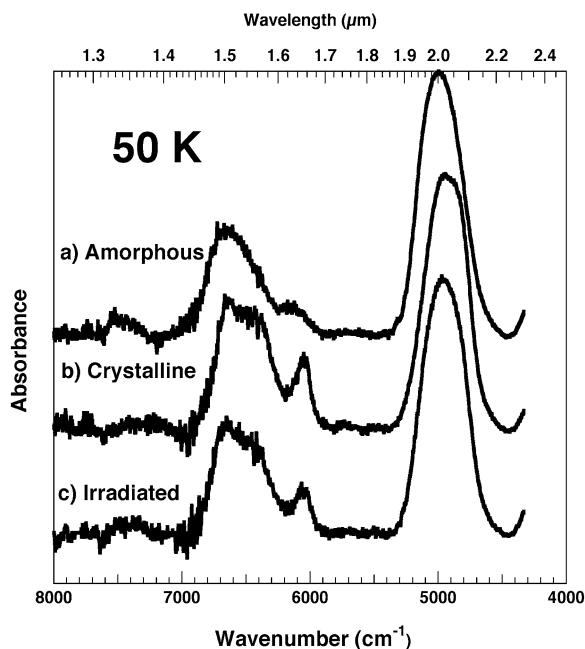


Fig. 9. Absorbance spectra of an H₂O–ice sample deposited at 50 K (a), heated to 160 K, and cooled to 50 K (b) before irradiating to a dose of 11 eV/molecule (c). Irradiation reduced the strength of the 1.65- μ m band, but did not completely eradicate it. The spectra are stacked for clarity.

measure amorphization, we show that by 11–16 eV/molecule the H₂O–ice is amorphized at 40 K and lower. The experiment at 50 K does not reach the amorphous line (Fig. 9). Meanwhile, the 70 K experiment shows that this method is not useful at high temperatures where the scatter in the results is high and the changes with dose are negligible. We omit the 100 K results for this reason.

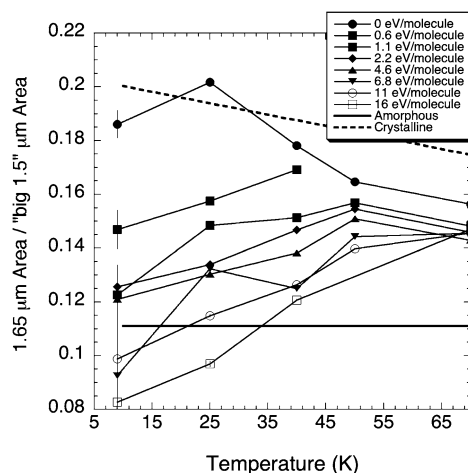


Fig. 10. The amorphization of crystalline H₂O–ice at low temperature, represented by the ratio of the areas of the 1.65- and “big 1.5”- μ m bands.

4. Discussion

We present the results of H₂O–ice amorphization experiments at a variety of temperatures in the wavelength range 1.0–2.5 μ m. As previously shown (Leto and Baratta, 2003; Moore and Hudson, 1992; Strazzulla et al., 1992), the low temperature irradiation experiments were the most effective at making the crystalline–ice spectrum look like that of amorphous H₂O–ice. We have also shown that a simple measurement can be used to differentiate between amorphous and crystalline phase, and also to identify partially irradiated ices. We provide this as a helpful tool to astronomers to interpret observations of icy Solar System objects.

One remaining question is how irradiation is affecting the infrared features. In order to weaken and broaden infrared absorptions, irradiation must break the hydrogen bonds, move or break the O–H bonds, or produce new compounds with new spectral features. If the peaks of the new compounds are similar to those of H₂O, then no change would be detectable. However, as O–H bonds are broken, there will be fewer H₂O molecules contributing to the vibrational modes, again weakening the bands. No new absorptions were produced in the NIR, therefore no new compounds were identified spectroscopically.

We would also like to explain the temperature dependence of the amorphization process. Some speculate that the free hydrogen is trapped in the H₂O–ice lattice up to 70 K (Strazzulla et al., 1991b). Above that temperature the hydrogen is free to move around and fill empty lattice sites. However, this temperature is too high to retain significant amounts of free hydrogen in the ice. The temperature dependence of amorphization varies between different experiments (Moore and Hudson, 1992; Strazzulla et al., 1992). Amorphization of H₂O–ice is undetectable in the 44- and 62- μ m features at 77 K, while it is still significant at 77 K and detectable in the 3.07- and 3.1- μ m bands at 100 K. This could be interpreted as a dependence on spectral range, however this experiment has the same temperature dependence as the FIR, while recent results in the NIR show complete amorphization at 90 K (Leto et al., 2005). The only difference in NIR and FIR experiments is the thickness

of the sample: $\sim 8\text{-}\mu\text{m}$ thick in this experiment and $4\text{-}\mu\text{m}$ thick in Moore and Hudson's (1992) experiment. The thickness of the sample would change the ability of free molecules to escape since the thicker the sample, the longer the path to escape. Therefore, in this experiment fewer of these materials might be able to escape. This may simply mean that the temperature dependence is linked to the laboratory set-up and/or radiation source, so we do not have a hard upper bound on temperature of amorphization in the real world. Further measurements need to be made to determine the bounds of amorphization's temperature dependence before we can determine the full extent of this process in the Solar System.

Our results are only applicable to Solar System objects with surface temperatures lower than 50 K. This rules out icy satellites, but includes Kuiper belt objects. To estimate a timescale to amorphization on icy Solar System objects, we need to balance it with other relevant processes including sublimation, spallation, radiation induced chemistry, and resurfacing due to impacts, tectonism or cryo-vulcanism. Ignoring all processing except for amorphization, the surface of a Kuiper belt object, would reach a dose of $\sim 10\text{ eV/molecule}$ in 10^3 years in the first $0.1\text{ }\mu\text{m}$ of the surface, but may take as long as 10^8 years to process to a significant depth (Cooper et al., 2003). The collision rate for 100-km radius Kuiper belt objects has been calculated to be roughly $10^7\text{--}10^8$ years (Durda and Stern, 2000), but may be significantly longer (Bernstein et al., 2004). This still leaves several processes that have no time constraint. That being said, Jewitt and Luu (2004) conclude that the surface of Quaoar is fresh, due to the presence of crystalline H₂O-ice, and our results agree with this assessment.

Acknowledgments

The authors thank Marla Moore and Reggie Hudson for making this project possible, and Robert Ferrante for technical advice. We thank Steve Brown and members of the GSFC/Radiation Facility for operation of the accelerator. Mastrapa thanks Max Bernstein for thoughtful comments on the manuscript and the NASA Ames Astrochemistry group for technical and software support. Mastrapa also thanks two anonymous reviewers for their very rapid responses, which were detailed, thoughtful, and constructive.

References

- Bednarek, J., Plonka, A., Hallbrucker, A., Mayer, E., 1998. Radical generation upon gamma-irradiation of two amorphous and two crystalline forms of water at 77 K. *J. Phys. Chem. A* 102, 9091–9094.
- Bernstein, M.P., Dworkin, J.P., Sandford, S.A., Cooper, G.W., Allamandola, L., 2002. Racemic amino acids from the ultraviolet photolysis of interstellar ice analogues. *Nature* 416, 401–403.
- Bernstein, G.M., Trilling, D.E., Allen, R.L., Brown, M.E., Holman, M., Malhotra, R., 2004. The size distribution of trans-neptunian bodies. *Astron. J.* 128, 1364–1390.
- Bertie, J.E., Whalley, E., 1964. Infrared spectra of ice *Ih* and *Ic* in the range 4000 to 350 cm^{-1} . *J. Chem. Phys.* 40, 1637–1645.
- Bertie, J.E., Whalley, E., 1967. Optical spectra of orientationally disordered crystals. II. Infrared spectrum of ice *Ih* and ice *Ic* from 360 to 50 cm^{-1} . *J. Chem. Phys.* 46, 1271–1284.
- Brown, W.L., and 9 colleagues, 1982. Erosion and molecule formation in condensed gas films by electronic energy loss of fast ions. *Nucl. Instrum. Methods* 198, 1–8.
- Ciavola, G., Foti, G., Torrì, L., Pirronello, V., Strazzulla, G., 1982. Molecular erosion of ice by keV ion bombardment. *Radiat. Eff.* 65, 167–172.
- Clark, R.N., 1981. Water frost and ice: The near-infrared spectral reflectance 0.625–2.5 μm . *J. Geophys. Res.* 86, 3087–3096.
- Cooper, J.F., Christian, E.R., Richardson, J.D., Wang, C., 2003. Proton irradiation of Centaur, Kuiper belt, and Oort cloud objects at plasma to cosmic ray energy. *Earth Moon Planets* 92, 261–277.
- Cruikshank, D.P., Brown, R.H., Calvin, W.M., Roush, T.L., Bartholomew, M.J., 1998. Ices on the satellites of Jupiter, Saturn, and Uranus. In: Schmitt, B., de Bergh, C., Festou, M. (Eds.), *Solar System Ices*. Kluwer Academic, Norwell, MA, pp. 655–684.
- Durda, D.D., Stern, S.A., 2000. Collision rates in the present-day Kuiper belt and Centaur regions: Applications to surface activation and modification on comets, Kuiper belt objects, Centaurs, and Pluto-Charon. *Icarus* 145, 220–229.
- Fink, U., Larson, H.P., 1975. Temperature dependence of the water-ice spectrum between 1 and 4 microns: Application to Europa, Ganymede, and Saturn's rings. *Icarus* 24, 411–420.
- Gerakines, P.A., Schutte, W.A., Greenberg, J.M., van Dishoeck, E.F., 1995. The infrared band strengths of H₂O, CO, and CO₂ in laboratory simulations of astrophysical ice mixtures. *Astron. Astrophys.* 296, 810–818.
- Gerakines, P.A., Bray, J.J., Davis, A., Richey, C.R., 2005. The strengths of near-infrared absorption features relevant to interstellar and planetary ices. *Astrophys. J.* 620, 1140–1150.
- Grundy, W.M., Schmitt, B., 1998. The temperature-dependent near-infrared absorption spectrum of hexagonal H₂O ice. *J. Geophys. Res.* 103, 25809–25822.
- Hagen, W., Tielens, A.G.G.M., 1982. The librational region in the spectrum of amorphous solid water and ice *Ic* between 10 and 140 K. *Spectrochim. Acta* 38A, 1089–1094.
- Hagen, W., Tielens, A.G.G.M., Greenberg, J.M., 1981. The infrared spectra of amorphous solid water ice and ice *Ic* between 10 K and 140 K. *Chem. Phys.* 56, 367–379.
- Hapke, B., Wells, E., Wagner, J., Partlow, W., 1981. Far-UV, visible, and near-IR reflectance spectra of frosts of H₂O, CO₂, NH₃, and SO₂. *Icarus* 47, 361–367.
- Hase, H., Kawabata, K., 1976. Trapped electrons in crystalline D₂O ice at 4 K. *J. Chem. Phys.* 65, 64–67.
- Heavens, O.S., 1991. *Optical Properties of Thin Films*. Dover, New York.
- Hudgins, D., Sandford, S.A., Allamandola, L.J., Tielens, A.G.G.M., 1993. Mid- and far-infrared spectroscopy of ices: Optical constants and integrated absorptions. *Astrophys. J. Suppl. Ser.* 86, 713–870.
- Hudson, R.L., Moore, M.H., 1992. A far-IR study of irradiated ice: An unreported oscillation between amorphous and crystalline phases. *J. Phys. Chem.* 96, 6500–6504.
- Jenniskens, P., Blake, D.F., 1994. Structural transitions in amorphous water ice and astrophysical implications. *Science* 265, 753–756.
- Jenniskens, P., Blake, D.F., Wilson, M.A., Pohorille, A., 1995. High-density amorphous ice, the frost on interstellar grains. *Astrophys. J.* 455, 389–401.
- Jenniskens, P., Banham, S.F., Blake, D.F., McCoustra, M.R.S., 1997. Liquid water in the domain of cubic crystalline ice *Ic*. *J. Chem. Phys.* 107, 1232–1241.
- Jenniskens, P., Blake, D.F., Kouchi, A., 1998. Amorphous water ice. A Solar System material. In: Schmitt, B., de Bergh, C., Festou, M. (Eds.), *Solar System Ices*. Kluwer Academic, Norwell, MA, pp. 139–156.
- Jewitt, D.C., Luu, J., 2004. Crystalline water ice on the Kuiper Belt Object (50000) Quaoar. *Nature* 432, 731–733.
- Johnson, R.E., 1982. *Introduction to Atomic and Molecular Collisions*. Plenum Press, New York.
- Johnson, J.E., Moulton, G.C., 1978. ESR study of ice irradiated at 42 K, a thermally reversible radical. *J. Chem. Phys.* 69, 3108–3111.
- Kouchi, A., Kuroda, T., 1990. Amorphization of cubic ice by ultraviolet irradiation. *Nature* 344, 134–135.
- Kouchi, A., Yamamoto, T., Kozasa, T., Kuroda, T., Greenberg, J.M., 1994. Conditions for condensation and preservation of amorphous ice and crystallinity of astrophysical ices. *Astron. Astrophys.* 290, 1009–1018.

- Leto, G., Baratta, G.A., 2003. Ly-alpha photon induced amorphization of *Ice* water ice at 16 Kelvin. Effects and quantitative comparison with ion irradiation. *Astron. Astrophys.* 397, 7–13.
- Leto, G., Gomis, O., Strazzulla, G., 2005. The reflectance spectrum of water ice: Is the 1.65 μm msp peak a good temperature probe? *Mem. Soc. Astron. Ital. Suppl.* 6, 57–62.
- McDonald, G.D., Whited, L.J., DeRuiter, C., Khare, B.N., Patniak, A., Sagan, C., 1996. Production and chemical analysis of cometary ice tholins. *Icarus* 122, 107–117.
- Moore, M.H., Hudson, R.L., 1992. Far-infrared spectral studies of phase changes in water ice induced by proton irradiation. *Astrophys. J.* 401, 353–360.
- Moore, M.H., Donn, B., Khanna, R., A'Hearn, M.F., 1983. Studies of proton-irradiated cometary-type ice mixtures. *Icarus* 54, 388–405.
- Northcliffe, L.C., Shilling, R.F., 1970. Range and stopping-power tables for heavy ions. *Nucl. Data Tables Sect. A* 7, 233–285.
- Ockman, N., 1958. The infra-red and Raman spectra of ice. *Adv. Phys.* 7, 199–220.
- Petrenko, V.F., Whitworth, R.W., 1999. *Physics of Ice*. Oxford Univ. Press, Oxford, UK.
- Reimann, C.T., Boring, J.W., Johnson, R.E., Garrett, J.W., Farmer, K.R., Brown, W.L., Marcantonio, K.J., Augustyniak, W.M., 1984. Ion-induced molecular ejection from D_2O ice. *Surface Sci.* 147, 227–240.
- Schmitt, B., Quirico, E., Trotta, F., Grundy, W.M., 1998. Optical properties of ices from UV to infrared. In: Schmitt, B., de Bergh, C., Festou, M. (Eds.), *Solar System Ices*. Kluwer Academic, Norwell, MA, pp. 199–240.
- Schutte, W.A., Allamandola, L., Sanford, S.A., 1993. Formaldehyde and organic molecule production in astrophysical ices at cryogenic temperatures. *Science* 259, 1143–1145.
- Siegel, S., Flournoy, J.M., Baum, L.H., 1961. Irradiation yields of radicals in gamma-irradiated ice at 4.2 and 77 K. *J. Chem. Phys.* 34, 1782–1788.
- Smith, R.G., Robinson, G., Hyland, A.R., Carpenter, G.L., 1994. Molecular ices as temperature indicators for interstellar dust: The 44- and 62- μm lattice features of H_2O ice. *Mon. Not. R. Astron. Soc.* 271, 481–489.
- Stern, S.A., 2003. The evolution of comets in the Oort cloud and Kuiper belt. *Nature* 424, 639–642.
- Strazzulla, G., Baratta, G.A., Johnson, R.T., Donn, B., 1991a. Primordial comet mantle: Irradiation production of a stable, organic crust. *Icarus* 91, 101–104.
- Strazzulla, G., Leto, G., Baratta, G.A., Spinella, F., 1991b. Ion irradiation experiments relevant to cometary physics. *J. Geophys. Res.* 96, 17547–17552.
- Strazzulla, G., Baratta, G.A., Leto, G., Foti, G., 1992. Ion-beam-induced amorphization of crystalline water ice. *Europhys. Lett.* 18, 517–522.
- Sugisaki, M., Suga, H., Seki, S., 1969. Calorimetric study of glass transition of the amorphous ice and of the phase transformation between the cubic and hexagonal ices. In: Riehl, N. (Ed.), *Physics of Ice*. Plenum Press, New York, pp. 329–343.
- Watanabe, N., Horii, T., Kouchi, A., 2000. Measurements of D_2 yields from amorphous ice by ultraviolet irradiation at 12 K. *Astrophys. J.* 541, 772–778.
- Whalley, E., 1977. A detailed assignment of the O–H stretching bands of ice I. *Can. J. Chem.* 55, 3429–3441.